PHYSICAL REVIEW B VOLUME 8, NUMBER 8 15 OCTOBER 1973

Intensity-Energy Spectra for Nickel Using an Exact Multiple-Scattering Method with Layer-Dependent Vibration Amplitudes*

S. Y. Tong
Department of Physics, North Dakota State University, Fargo, North Dakota 58102
and Department of Physics, University of Wisconsin-Milwaukee, Milwaukee, Wisconsin 53201

L. L. Kesmodel
Department of Physics, University of Texas, Austin, Texas 78712
(Received 4 June 1973)

Intensity-energy spectra are calculated for the specular and nonspecular beams on the (001) and (110) faces of nickel for a wide range of incident angles and energies between 0 and 200 eV. Calculations are done using a rigid-lattice model and a finite-temperature model with layer-dependent vibration amplitudes for the surface layers. It is found that good agreement is obtained between room-temperature calculated results and experiment in peak positions, peak widths, and angular evolution of the profiles on both faces of nickel. The rigid-lattice model gives calculated absolute reflectivities about four times too high compared to experiment at energies above 100 eV on the (001) face. However, room-temperature calculated results agree well with experiment in absolute reflectivities on both the (001) and (110) faces. A single inner potential places calculated peak positions in good agreement with experiment on both Ni (001) and Ni (110). Results of this work and other recent calculations on nickel provide a useful and complete set of spectra analyses for clean faces of a transition metal.

I. INTRODUCTION

Recently there has been considerable interest in the systematic comparison between theory and experiment of elastic low-energy-electron-diffraction (LEED) spectra on single faces of different materials. Intensity-energy (IV) spectra are calculated and compared with experiment for many angles of incidence in a wide energy range. The comparisons are done for a number of reflected beams and for different faces of a given material.[1-6] The advantages of such systematic comparisons are manifold. (i) They provide a good test of the dynamical factors used in the theoretical models. The same set of dynamical factors must describe observed IV profiles for many incident angles, different reflected beams, and on different crystal faces. Dynamical factors chosen to fit measured spectra for limited prescribed conditions (i.e., incident angle, crystal face, etc.) but which fail to describe more extended conditions are of limited use only. (ii) A systematic comparison between theory and experiment on different crystal faces can help detect peculiarities on some faces. If a set of dynamical factors gives good agreement between theory and experiment for different angles and different beams on one crystal face but gives poor agreement on another crystal face, this suggests the possible presence of surface defects on the latter face. The surface defects may be in the forms of surface contaminants, surface steps, or reordering of surface crystal structures. There can also be expansion or contraction of top surface layers. (iii) Comparisons between theory and experiment for a range of incident angles provide valuable information on the evolution of the IV profiles as a function of incident angle. This information is particularly useful in discriminating between different crystal potentials. At normal or close to normal angles of incidence, the IV spectra are not sensitive to details in the crystal potentials. This is because the reflected beams at close to normal incidence have high geometric symmetries. But if one looks at the systematic angular evolution of LEED profiles for a wide range of incident angles, differences in crystal potentials become important. A direct comparison of effects produced by two different potentials of nickel is reported elsewhere.[5]

Recently, detailed comparisons between theory and experiment have been applied to three faces of aluminum[1-3] [i.e., the (001), (110), and (111) faces]. This was possible partly because of the available systematic experimental data by Jona.[7] It was found that while theory and experiment agree rather well on the (001) and (111) faces, the agreement on the (110) face is not as good, especially in the matching of peak positions.[1-3] Comparisons of absolute reflectivities were not made because the data were taken in arbitrary relative intensities. Another material worth considerable attention is metallic nickel,[4-6,8-10] which is a transition metal. Recently, a systematic set of experimental data was taken on three faces of nickel in a wide energy range between 0 and 240 eV.[10-12] The data were taken in absolute reflectivities. Comparisons between theory and experiment can now be made in

absolute reflectivities on different faces of nickel. Nickel is a substance active in chemisorption. A number of gas species form ordered overlayers on single faces of nickel. The analysis of LEED spectra on clean nickel surfaces is a prerequisite for theoretical studies of chemisorbed systems on the material.[13–15]

Besides the determination of surface structures of chemisorbed systems, there is also considerable current interest in the study of surface vibration properties on different crystal faces.[16–22] Such studies provide information on the force constants between ion cores at the surface. Because surface atoms are more loosely bound, their vibration amplitudes are generally larger than those in the bulk. Calculations show that surface atoms vibrate with mean-square displacement amplitudes two or three times larger than their counterparts in the bulk.[18–22] These calculations also show that the surface vibration amplitudes decrease gradually into the bulk, reaching bulk values at approximately five atomic layers. In this work, we apply an exact multiple-scattering method to calculate elastic *IV* spectra for different faces of clean nickel. We compare our results with recent experimental data taken by Demuth and co-workers[10–12] and Andersson and Kasemo.[23,24] Other experimental data are also available on nickel.[25–29] A comprehensive discussion comparing existing experimental work on nickel is given in Ref. 11. In our calculations, a microscopic model using layer-dependent vibration amplitudes for different surface layers is used. The organization of the remainder of this paper is as follows. In Sec. II we describe the model of our method. In Secs. III and IV we present comparisons between theory and experiment for clean faces of nickel. Finally, in Sec. V we give a summary and discussion of this work.

II. COMPUTATION MODEL

The theoretical model used in this work for calculating *IV* spectra on different faces of nickel is based on an exact multiple-scattering method proposed by Beeby.[30] In this method, the crystal potential and electron propagators are expanded in spherical-partial-wave components. Multiple-scattering events in each atomic layer are then summed exactly.[2,4,30–32] This is done by inverting a $\bar{l}^2\times\bar{l}^2$ complex matrix, where $\bar{l}=l+1$ is the number of partial waves included in the calculation. The resulting planar matrix $\tau_n^{LL'}(k_0)$ is then used to evaluate the total scattering matrix $T_n^{LL'}(k_0)$ which includes both interlayer and intralayer multiple-scattering events. Here, n is the layer index and $L=(l, m)$. The matrix equations satisfied by $\tau_n^{LL'}(k_0)$ and $T_n^{LL'}(k_0)$ are, respectively,[2,30,32]

$$\tau_n^{LL'}(k_0)=t_n^L(k_0)\delta_{LL'}+\sum_{L_1} t_n^L(k_0)G_{LL_1}^{SP}(\vec{k}_i)\tau_n^{L_1L'}(k_0) \quad (1)$$

and

$$T_n^{LL'}(k_0)=\tau_n^{LL'}(k_0)+\sum_{L_1L_2}\tau_n^{LL_1}(k_0)\times\sum_{n'\neq n}G_{L_1L_2}^{nn'}(\vec{k}_i)T_{n'}^{L_2L'}(k_0)\,. \quad (2)$$

Explicit expressions for the planar and interplanar electron propagators $G_{LL'}^{SP}(\vec{k}_i)$ and $G_{LL'}^{nn'}(\vec{k}_i)$ are given elsewhere.[1,2,30] In Eq. (1), $t_n^L(k_0)$ is a layer-dependent diagonal matrix for single ion-core scattering. Equation (2) for $T_n^{LL'}(k_0)$ can be solved for a finite number of atomic layers. The dimension of the complex matrix to be inverted is $N\bar{l}^2\times N\bar{l}^2$, where N is the number of layers included in the calculation. In this work, we take $N=5$ atomic layers.

At finite temperatures, the single ion-core scattering matrix $t_n^L(k_0)$ is related to the rigid-lattice scattering matrix $t_{n0}^l(k_0)$ by[1]

$$t_n^L(k_0)=\exp(-\langle U_n^2\rangle_T k_0^2)\sum_{l_1l_2}a(l_1l_2l;\,000)\times\left(\frac{4\pi(2l_1+1)(2l_2+1)}{2l+1}\right)^{1/2}t_{n0}^{l_1}(k_0)i_{l_2}(\langle U_{n'}^2\rangle_T k_0^2)\,, \quad (3)$$

where $\langle U_n^2\rangle_T$ is an averaged mean-square displacement amplitude for the nth layer. The average is taken over different vibration directions. One may use the present microscopic method to calculate the temperature dependence of *IV* spectra and determine values of $\langle U_n^2\rangle_T$ for each atomic layer.[33] In this work, we deal mainly with room-temperature *IV* profiles and for simplicity we use calculated values of $\langle U_n^{z2}\rangle_T$ as inputs in our calculations. The rigid-lattice scattering matrix $t_{n0}^l(k_0)$ is given in terms of energy-dependent phase shifts $\delta_l(E)$ by[1,30,31]

$$t_{n0}^l(k_0)=\frac{-\hbar^2}{2m}[e^{2i\delta_l(E)}-1]/2ik_0\,. \quad (4)$$

In Eq. (4), the phase shifts $\delta_l(E)$ are taken to be independent of atomic layer. The expansion in Eq. (3) is given in terms of modified spherical Bessel functions of the first kind $i_l(X)$.[1,2,34] In this work, we include up to $\bar{l}=\bar{l}_1=5$ and $\bar{l}_2=9$. Thus, taking five atomic layers and five phase shifts, the final dimension of $T_n^{LL'}(k_0)$ in Eq. (2) is $125\times125\times2$. The factor of 2 comes from the fact that $T_n^{LL'}(k_0)$ is a complex matrix. Calculated values of $\langle U_n^{z2}\rangle_T$ for the (001) and (110) faces of nickel are shown in Fig. 1 as a function of atomic layer.[18] A bulk Debye temperature

$$\Theta_D^B=\left(\frac{3\hbar^2T}{Mk_B\langle U_B^2\rangle_T}\right)^{1/2}$$

of 440 °K is used in this work. The absolute reflectivity for the $\vec{g}_0$th reflected beam is given by[1]

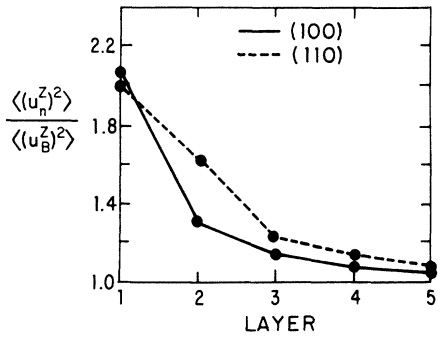

FIG. 1. Mean-square displacement amplitudes in the direction normal to the surface as a function of atomic layer. The calculated results are taken from Ref. 18. The solid line is for the (001) face and the broken line is for the (110) face.

$$R(\vec{g}_0, E) = \frac{k_{\perp}^{\text{out}}(\vec{g}_0)}{k_{i\perp}^{\text{out}}}\left(\frac{2m}{\hbar^2}\right)^2\left(\frac{8\pi^2}{A}\right)^2\left|\frac{S_{\vec{g}_0}(\vec{k}_f, \vec{k}_i)}{k_{\perp}(\vec{g}_0)}\right|^2 , \tag{5}$$

where[2,4,32]

$$S_{\vec{g}_0}(\vec{k}_f, \vec{k}_i) = \sum_n \exp[i(\vec{k}_i - \vec{k}_f)\cdot\vec{d}_n] \times \sum_{LL'} Y_L(\vec{k}_f)Y_{L'}^*(\vec{k}_i)T_n^{LL'}(k_0) \tag{6}$$

and

$$\vec{k}_{f\parallel} = \vec{k}_{i\parallel} + \vec{g}_0 . \tag{7}$$

At finite temperatures, using five inequivalent layer-vibration amplitudes and five phase shifts, the calculation takes an average of 31 sec per energy point for five reflected beams on the (001) face and 35 sec per energy point for six reflected beams on the (110) face. The computations are done on a CDC 6600 machine at the University of Texas, Austin. Over 50% of the computation time is used in the final matrix inversion to obtain the complex matrix $T_n^{LL'}(k_0)$. Computation time increases with energy due to the larger number of planar unit cells and Bloch waves one must include in the intraplanar and interplanar sums, respectively, in order to obtain convergence at higher energies. For the planar sums, a great deal of time is saved by expressing sums over four gradrants into sums over the first quadrant alone. A total equivalent of 14 400 planar unit cells (3600 planar unit cells per quadrant) are allowed in the planar sums, but a cutoff is set at an accuracy of 10^{-4}. With this cutoff value, a maximum of about 4000 planar unit cells (1000 planar unit cells per quadrant) are actually used in the calculations in the energy range considered. Interplanar sums are done in reciprocal space over a possible total of 169 Bloch waves with cutoff set at 10^{-3}. With this cutoff value, about 60 Bloch waves are actually needed at high energies on the (110) face for good convergence. Computation times vary slightly on different crystal faces because sizes of planar unit cells and magnitudes of Bloch waves differ on different faces. The computations require a computer core storage of 55K 60-bit words (approximately equal to 440K bytes). About 70% of this core storage is used in storing the complex matrix $T_n^{LL'}(k_0)$.

The crystal potential used in this work is a self-consistent Hartree-Fock-Slater potential constructed by Wakoh.[35] Energy-dependent phase shifts are obtained from this potential. We show in Fig. 2 the first six phase shifts in the energy range 0–200 eV. The energy scale here is measured with respect to the muffin-tin average. In our calculations, the $l \geq 5$ partial waves are neglected. Note that for nickel, unlike the case of aluminum, the $l = 2$ partial wave is small in the entire energy range and the $l = 3$ partial wave is dominant above 70 eV. Previously, we have calculated intensity-energy spectra for nickel[8,10] using an exact Hartree-Fock potential constructed by Pendry.[13,36] Comparisons of LEED-spectra results for nickel using the two different crystal potentials are given elsewhere.[5] The value of electron damping in nickel is somewhat uncertain. Previous calculations used values of electron self-energy Σ_2 ranging from 3[13,37] to 6.5 eV.[8,10] Recently, Demuth *et al.*[6] suggested a self-energy model for nickel with an energy dependence of $E^{1/3}$. In Figs. 3 and 4 we show intensity-energy spectra results for the specular beam on Ni(001) at $\theta = 0°$ and 6°, $\varphi = 45°$ using two models of electron self-energy.

In model A, we use the prescription proposed by Demuth *et al.*[6] and set $\Sigma_2(E) = 3.8[(E + V_0)/104]^{1/3}$ eV. Here, V_0 is the value of the inner potential

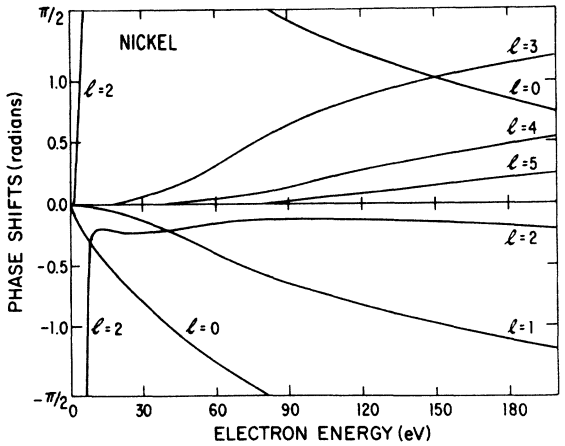

FIG. 2. First six phase shifts of nickel in the energy range 0–200 eV measured from the muffin-tin average. The crystal potential is taken from Ref. 35.

and E is the incident energy measured from the vacuum level. In this model, a constant inner potential of $V_0 = 14$ eV is used on both faces of nickel. The value of $\Sigma_2(E)$ varies from 2.48 eV at $E = 15$ eV to 4.83 eV at $E = 200$ eV. In model B, a constant value of $\Sigma_2(E) = 3.6$ eV is used. From the comparisons shown in Figs. 3 and 4, it is concluded that model A gives slightly better ratios in relative peak heights between low- and high-energy peaks. Because of this, we use model A for the electron damping for most of the calculations reported in this work. A screening model in which the conduction electrons extend a distance d_z from the plane of centers of the surface ion cores is used.[1,8-10,31] This screening model is described in detail in Ref. 1. Other boundary and reflection conditions at the vacuum-solid interface used in this work are the same as those used earlier.[1,8-10,31] Intensity-energy spectra are calculated in the energy range 0–200 eV for Ni(001) and Ni(110) along two azimuthal directions and a wide range of polar angles. We limit ourselves to energies below 200 eV in this work because at higher energies it is no longer enough to include only five partial waves in the calculation.

III. INTENSITY-ENERGY SPECTRA ON Ni(001)

In this section we present intensity-energy spectra results on Ni(001) for the specular and nonspecular beams. The convention used in this work for the azimuthal orientations and the nomenclature of nonspecular beams is based on the two-dimensional-surface unit cell. This convention differs from the space unit-cell convention used earlier by Jona[7] on the (001) face of aluminum. In particular, the $\varphi = 0°$ and 45° directions are interchanged in the two conventions. In Fig. 5 we show the positive directions of $\vec{k}_x$ and $\vec{k}_y$ and the nomenclature of nonspecular beams on the (001) and (110) faces of nickel defined in this work. In our convention, a right-handed coordinate system is used and $\vec{k}_z$ is positive towards the interior of the crystal.

The effects of room-temperature lattice vibrations on intensity-energy profiles are demonstrated in Fig. 6. Here, we compare the spectra for the (00) beam at $\theta = 6°$, $\varphi = 45°$ between the rigid-lattice model and the room-temperature calculation. For the latter calculation, five inequivalent layer-vibration amplitudes are used. From Fig. 6, we note that additional structures are evident in the spectra at high energies in the rigid-lattice model. Also, the calculated absolute reflectivities for the rigid-lattice model are about four times too high. The peak at $E = 100$ eV, for example, is about 1.2% (experiment), 1.7% (theory, $T = 300$ °K), and 4.25% (theory, rigid-lattice model). Results for two nonspecular beams at normal incidence are shown in Fig. 7. Again, the absolute reflectivities for the rigid-lattice calculations are too high. For the (01) beam, the peak at $E = 140$ eV, for example, is about 0.5% (experiment), 0.62% (theory, $T = 300$ °K), and 2.1% (theory, rigid-lattice model). For the (11) beam, the peak at $E = 115$ eV is about 0.2% (experiment), 0.26% (theory, $T = 300$ °K), and 0.7% (theory, rigid-lattice model). Thus, while room-temperature calculated results for absolute reflectivities agree well with experiment, results using the rigid-lattice model which do not include phonon contributions show additional structures at high energies and have absolute reflectivities too high by a factor of 3–4. The calculations shown in Figs. 6 and 7 are done using a constant damping of 3.6 eV. Room-temperature results using the damping model with a $E^{1/3}$ dependence[6] show slightly lower absolute reflectivities at $E \geq 100$ eV (see Fig. 10), but absolute reflectivities from the rigid-lattice model are still too high when compared with experiment.

Finite-temperature intensity-energy spectra for different beams in the $\varphi = 45°$ direction are calculated at $\theta = 0°$, 6°, 10°, 16°, and 20°. The damping model with a $E^{1/3}$ dependence[6] is used. Comparisons with experiment for the (00) beam at $\theta = 0°$ and 6° are already given in Figs. 3 and 4.

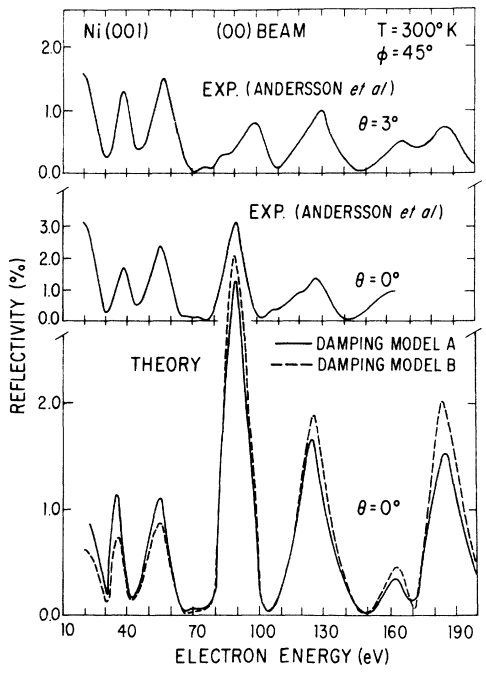

FIG. 3. Intensity-energy spectra for the (00) beam, Ni(001) at normal incidence and $T = 300$ °K. The solid line in the theory is for electron damping model A, the broken line is for electron damping model B. The experimental data are taken from Refs. 23 and 24. The energies are measured from the vacuum level.

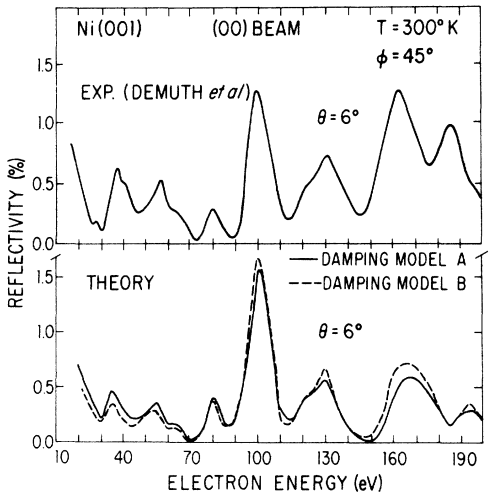

FIG. 4. Intensity-energy spectra for the (00) beam, Ni(001) at $\theta = 6°$, $\varphi = 45°$, and $T = 300$ °K. The solid line in the theory is for electron damping model A, the broken line is for electron damping model B. The experimental data are taken from Refs. 11 and 12. The energies are measured from the vacuum level.

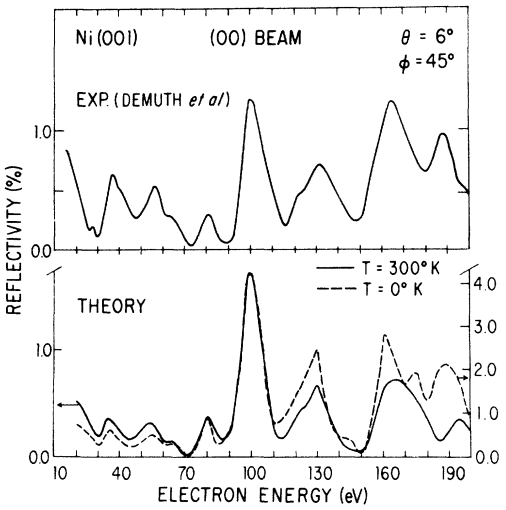

FIG. 6. Intensity-energy spectra for the (00) beam, Ni(001) at $\theta = 6°$ and $\varphi = 45°$. The solid line in the theory is for $T = 300$ °K, the broken line is for the rigid-lattice model. Note the different vertical scales corresponding to the two calculations. A constant electron self-energy of $\Sigma_2 = 3.6$ eV is used. The experimental data are taken from Refs. 11 and 12.

In Fig. 8 we show comparisons for the (00) beam at $\varphi = 45°$, $\theta = 10°$, 16°, and 20°. The experimental data of Demuth and co-workers[10–12] are used. We note that there is rather good agreement between theory and experiment in absolute reflectivities as well as in peak positions, peak widths, and angular evolution of the profiles. The agreement is good at small angles of incidence as well as at large incident angles. Intensities of the calculated peaks at higher energies (above $E \geq 150$ eV) are low compared to experiment, a fact also evident in other recent calculations of nickel.[4,6]

Results for the (00) beam at $\varphi = 0°$, $\theta = 6°$, 10°, and 20° are shown in Fig. 9. Again, there is good agreement in absolute reflectivities, peak positions, peak widths, etc., at small as well as at large angles. Results for two nonspecular beams at normal incidence are shown in Fig. 10. In the figure, we have included the data by Andersson and Kasemo[23,24] and Demuth and co-workers.[10–12] The two experimental data differ in measured absolute reflectivities by about a factor of 2. Calculated absolute reflectivities for the nonspecular beams at normal incidence using the present model of electron damping[6] and surface screening agree more closely to the absolute reflectivities measured by Andersson and Kasemo.[23,24]

Calculated *IV* spectra for nonspecular beams at off-normal angles of incidence in two azimuthal directions are shown in Figs. 11–14. The nomenclature of the beams follows the convention shown in Fig. 5. There is at present no experimental data available for these beams at off-normal incidence. This is partly because nonspecular beams move on the fluorescent screen as the incident energy is changed. This makes measurements of these beams rather difficult at off-normal incidence. The calculated profiles are presented here for future reference.

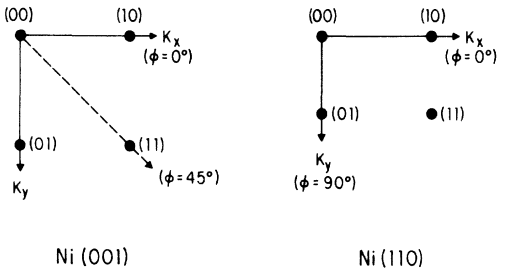

FIG. 5. Two-dimensional-surface unit-cell convention for azimuthal orientations and nomenclature of nonspecular beams on Ni(001) and Ni(110) faces.

IV. INTENSITY-ENERGY SPECTRA ON Ni(110)

We now turn to comparisons between theory and experiment on the (110) face of nickel. Intensity-energy profiles are calculated at room-temperature in the $\varphi = 90°$ direction at $\theta = 4°$, 8°, 16°, and 20°. The convention used for the azimuthal orientations is shown in Fig. 5. Results for the specular beam are shown in Fig. 15 compared with the experimental data by Demuth and co-workers.[10–12] From the figure we see that the splitting of the cal-

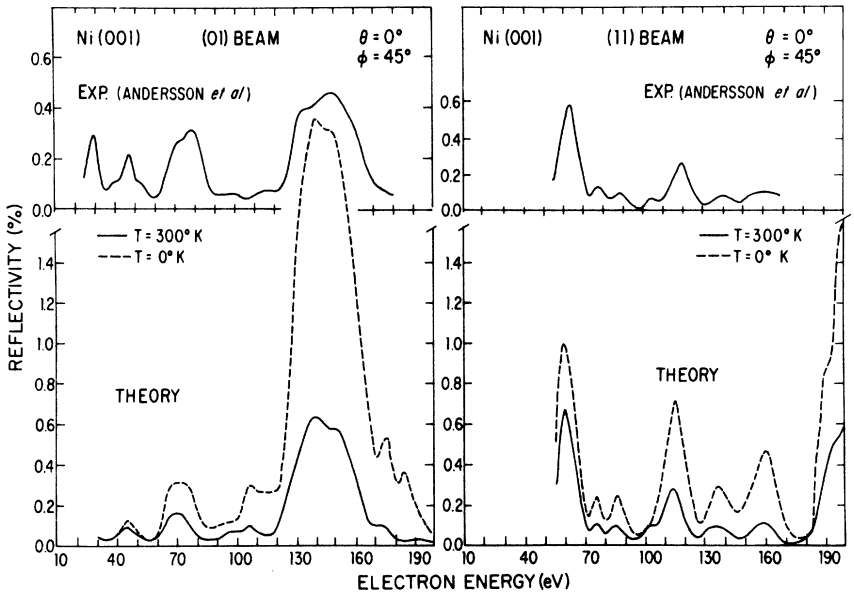

FIG. 7. Intensity-energy spectra for the (01) and (11) beams, Ni(001) at normal incidence. The solid lines in the theory are for $T = 300\,°K$, the broken lines are for the rigid-lattice model. A constant electron self-energy of $\Sigma_2 = 3.6$ eV is used. The experimental data are taken from Refs. 23 and 24.

culated peak at $\theta = 4°$, $E = 75$ eV is not as deep as that shown in the data. Also, the calculated secondary peaks at $E = 120$ eV, $\theta = 4°$ and 8° are low compared to those in experiment. One may think that this is because we have limited ourselves to only five partial waves in the calculation. However, recent results by Demuth and co-workers[6]

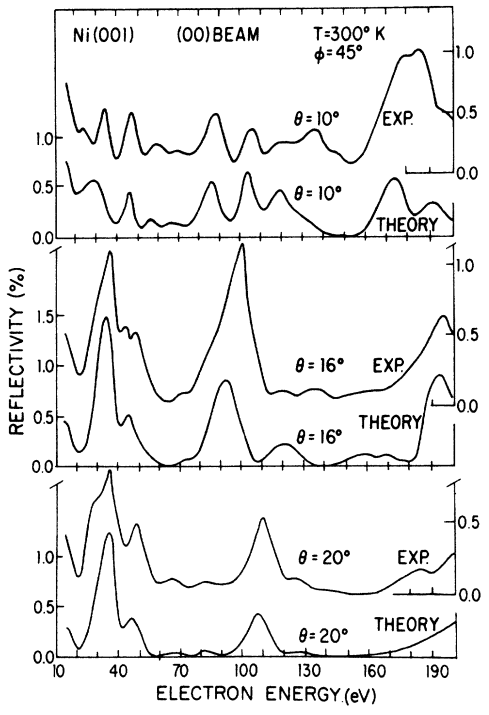

FIG. 8. Comparisons between theory and experiment of room-temperature intensity-energy spectra for the (00) beam, Ni(001) at $\varphi = 45°$, $\theta = 10°$, 16°, and 20°. The experimental data are taken from Refs. 10–12.

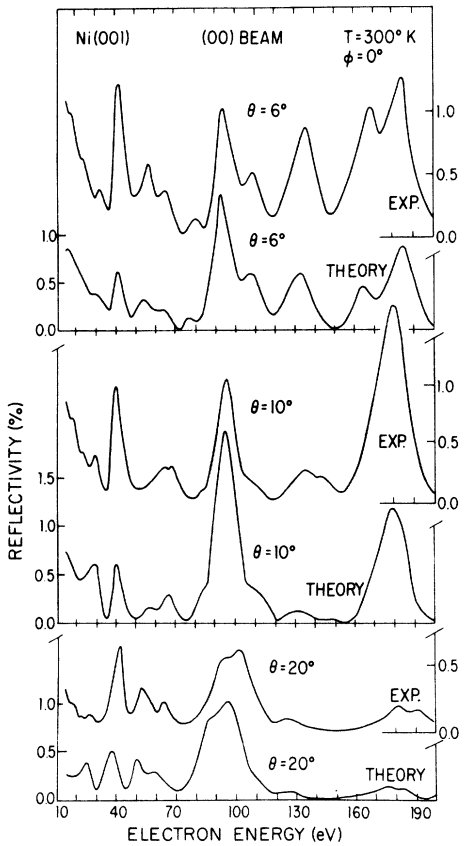

FIG. 9. Comparisons of room-temperature intensity-energy spectra for the (00) beam, Ni(001) at $\varphi = 0°$, $\theta = 6°$, 10°, and 20°. Other conditions are the same as in Fig. 8.

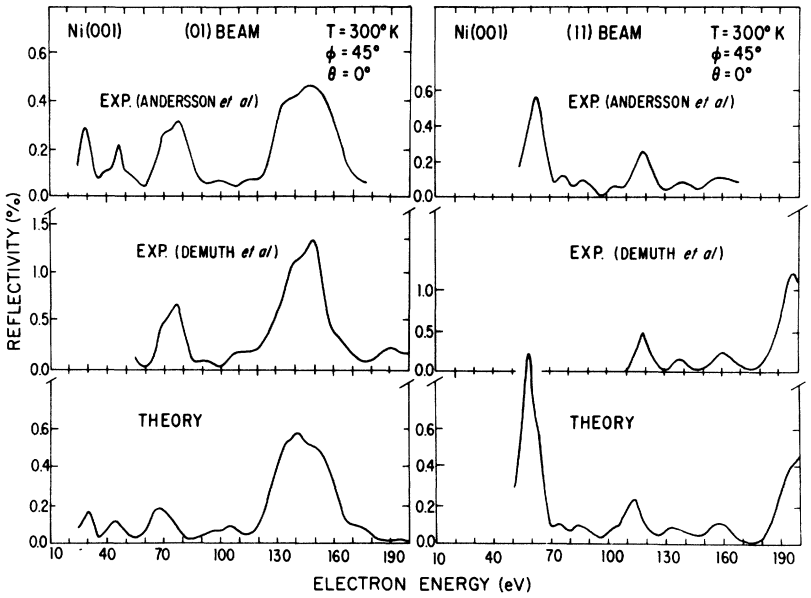

FIG. 10. Comparisons of room-temperature intensity-energy spectra for the (01) and (11) beams, Ni(001) at normal incidence.

using eight partial waves show very similar behavior. The agreement between theory and experiment improves at larger angles of incidence, and at $\theta = 20°$ the agreement becomes quite good. Also, unlike the case in aluminum,[1-3] peak positions agree well on both faces of nickel using a single inner potential of $V_0 = 14$ eV. Our findings here together with recent results from other calculations on nickel[4,6] indicate that a single inner potential would adequately place peak positions on all three faces [(100), (110), (111)] of nickel. Our results here also show that calculated reflectivities on the (110) face agree with experiment to the same degree of accuracy as those obtained on the (001)

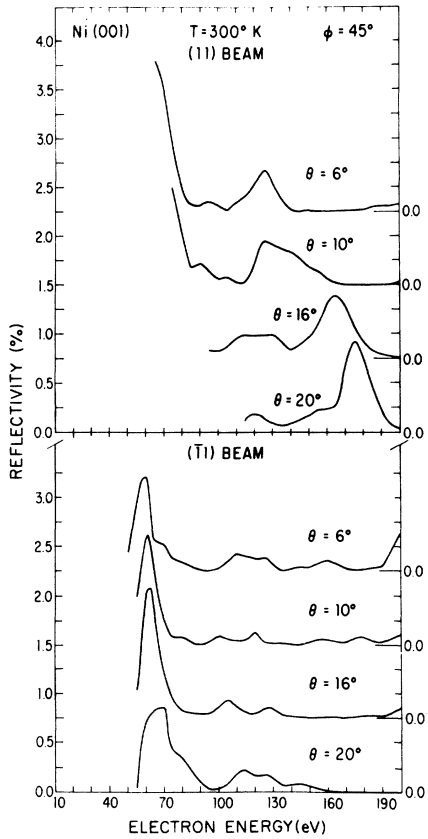

FIG. 11. Calculated results of room-temperature intensity-energy spectra for the (11) and ($\bar{1}$1) beams, Ni(001) at $\varphi = 45°$, $\theta = 6°$, 10°, 16°, and 20°.

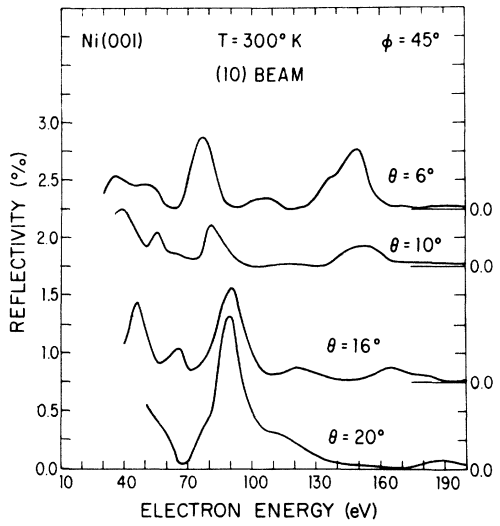

FIG. 12. Calculated results of room-temperature intensity-energy spectra for the (10) = (01) beams, Ni(001) at $\varphi = 45°$, $\theta = 6°$, 10°, 16°, and 20°.

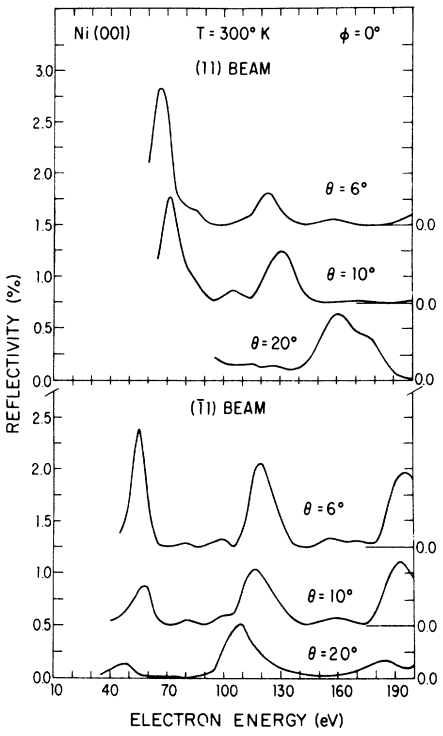

FIG. 13. Calculated results of room-temperature intensity-energy spectra for the (11) and ($\bar{1}$1) beams, Ni(001) at $\varphi = 0°$, $\theta = 6°$, 10°, and 20°.

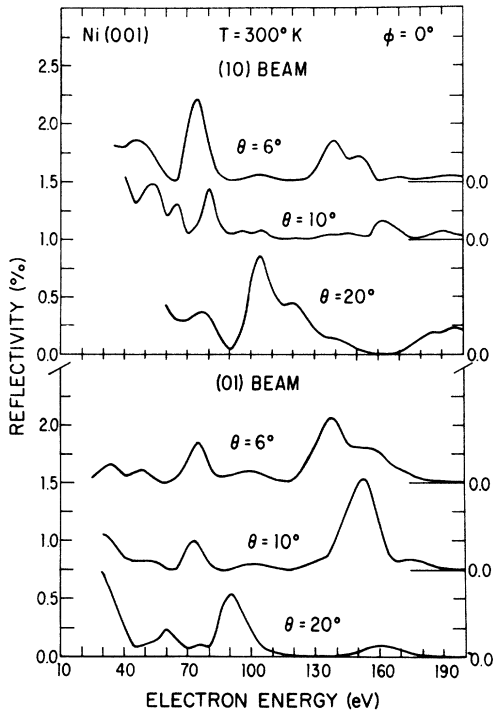

FIG. 14. Calculated results of room-temperature intensity-energy spectra for the (10) and (01) beams, Ni(001) at $\varphi = 0°$, $\theta = 6°$, 10°, and 20°.

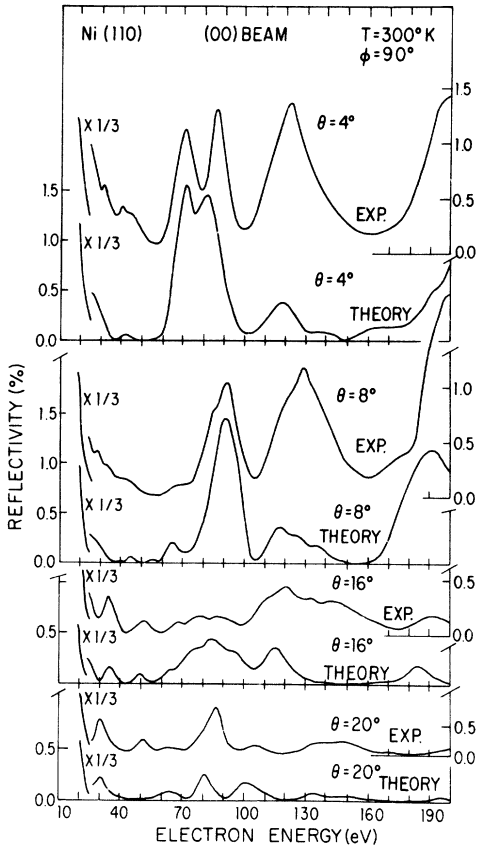

FIG. 15. Comparisons of room-temperature intensity-energy spectra for the (00) beam, Ni(110) at $\varphi = 90°$, $\theta = 4°$, 8°, 16°, and 20°. Other conditions are the same as in Fig. 8.

face. For example, the reflectivity for the split peak at $\theta = 4°$, $E = 75$ eV is about 1.3% in the data compared with 1.5% in the theory. To obtain the calculated reflectivities, the same dynamical model used for the (001) face is used for the (110) face. No additional adjustment is made in matching absolute reflectivities on the two faces.

Results for the specular beam along the $\varphi = 0°$ direction and $\theta = 4°$, 8°, and 20° are shown in Fig. 16. Again, for $\theta = 4°$ and 8° on this azimuth, the secondary peaks at $E = 120$ eV are too low in the calculated results. However, peak positions, peak widths, and absolute reflectivities all compare well with experiment. For example, the reflectivity of the peak at $\theta = 4°$, $E = 75$ eV is about 2.4% in the data and 2.9% in the calculation. The agreement between theory and experiment is again good at the large angle of incidence $\theta = 20°$.

Intensity-energy spectra for five nonspecular beams at normal incidence are shown in Figs. 17 and 18. There are good agreements between theory and experiment in peak positions, absolute reflectivities, and peak widths. For some beams, the

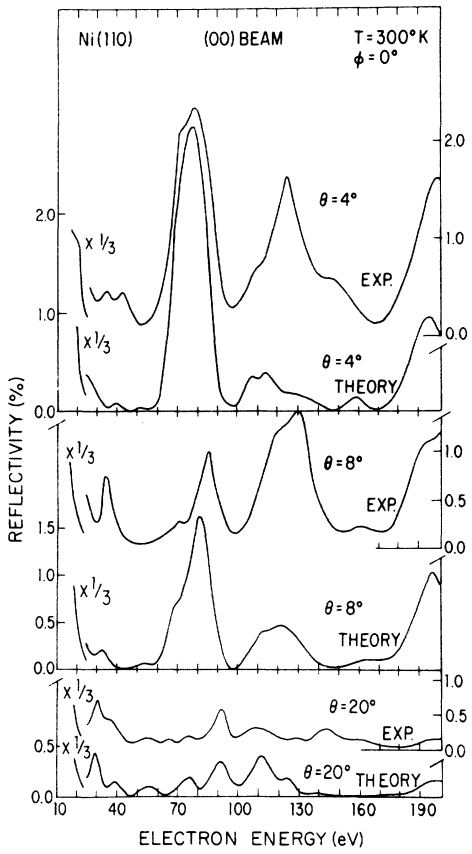

FIG. 16. Comparisons of room-temperature intensity-energy spectra for the (00) beam, Ni(110) at $\varphi = 0°$, $\theta = 4°$, 8°, and 20°. Other conditions are the same as in Fig. 8.

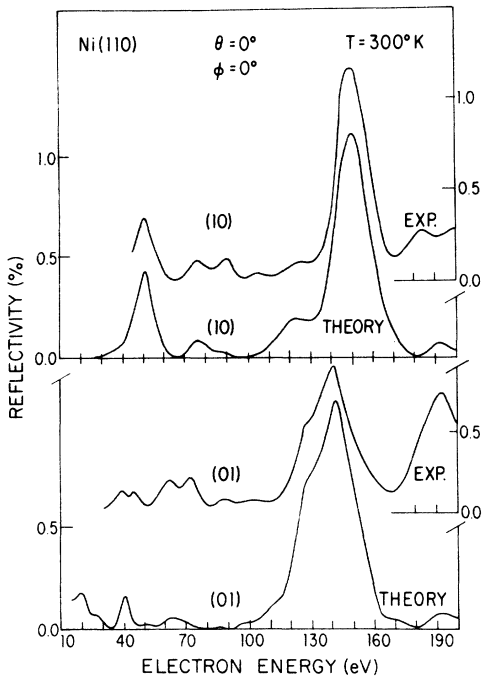

FIG. 17. Comparisons of room-temperature intensity-energy spectra for the (10), and (01) beams, Ni(110) at normal incidence.

experimental data start at rather high energies. This is because some nonspecular beams have large angles of reflection at low energies. Their reflected spots fall outside the fluorescent screen and hence are not measured. At higher energies, the angles of reflection decrease and measurements on these beams can be made. One may also apply a voltage bias to measure nonspecular beams at low energies but such a bias was not used in the experiments by Demuth and co-workers.[10–12]

Calculated results for the five nonspecular beams in two azimuthal directions at off-normal angles are shown in Figs. 19–23. Again, no experimental data are available on these beams at off-normal incidences and the calculated results are presented here mainly for future reference.

V. SUMMARY AND DISCUSSION

We have presented *IV* spectra results for Ni(001) and Ni(110) for a wide range of incident angles in the energy range 0–200 eV. Finite-temperature calculations are done using a dynamical model with five inequivalent layer-dependent mean-square vibration amplitudes. Comparisons with recent experiments by Demuth and co-workers[10–12] show good agreements in peak positions, peak widths, and angular evolution of the profiles. The agree-

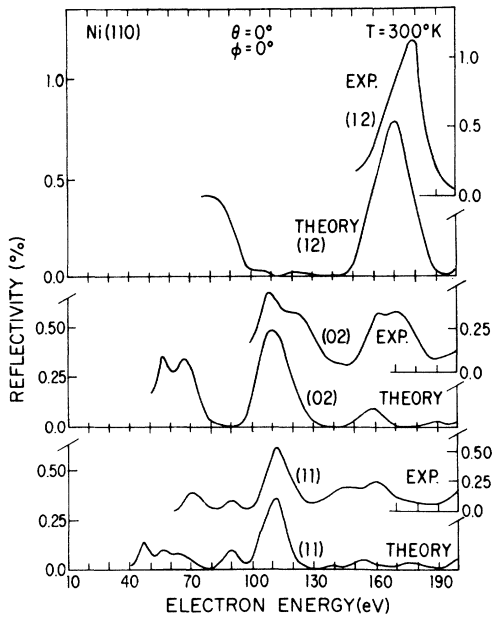

FIG. 18. Comparisons of room-temperature intensity-energy spectra for the (11), (02), and (12) beams, Ni(110) at normal incidence.

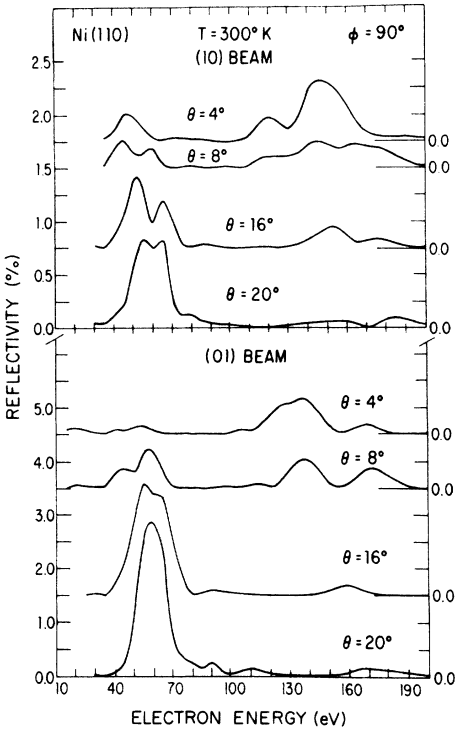

FIG. 19. Calculated results of room-temperature intensity-energy spectra for the (10) and (01) beams, Ni(110) at $\varphi = 90°$, $\theta = 4°$, 8°, 16°, and 20°.

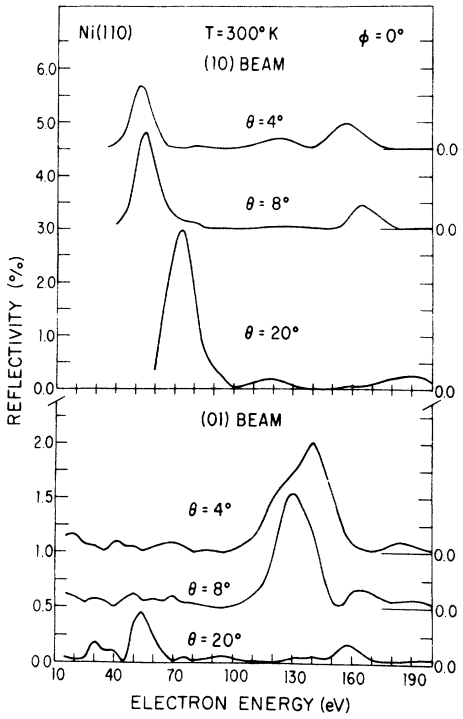

FIG. 21. Calculated results of room-temperature intensity-energy spectra for the (10) and (01) beams, Ni(110) at $\varphi = 0°$, $\theta = 4°$, 8°, and 20°.

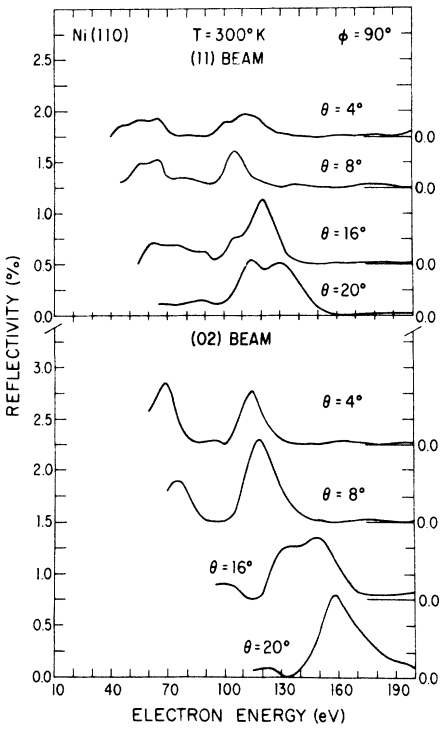

FIG. 20. Calculated results of room-temperature intensity-energy spectra for the (11) and (02) beams, Ni(110) at $\varphi = 90°$, $\theta = 4°$, 8°, 16°, and 20°.

ment is good at small angles as well as at large angles. A single inner potential places calculated

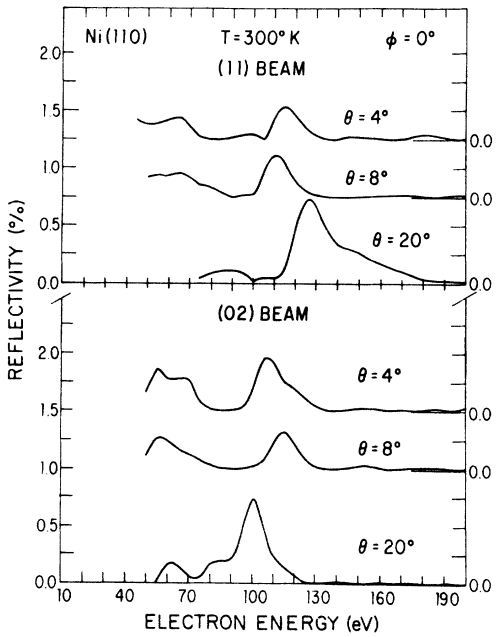

FIG. 22. Calculated results of room-temperature intensity-energy spectra for the (11) and (02) beams, Ni(110) at $\varphi = 0°$, $\theta = 4°$, 8°, and 20°.

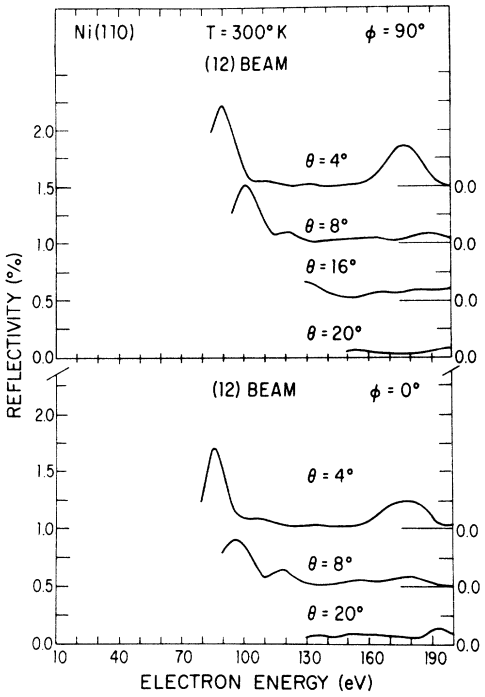

FIG. 23. Calculated results of room-temperature intensity-energy spectra for the (12) beam, Ni(110) at $\varphi = 90°$, $\theta = 4°$, 8°, 16°, 20° and at $\varphi = 0°$, $\theta = 4°$, 8°, 20°.

peaks in adequate agreement with experiment on both faces. This is rather unlike the case found for aluminum.[1-3]

Using the experimental data by Demuth and co-workers[10-12] we find the calculated absolute reflectivities agree well with experimental values on both faces of nickel. Recently, Laramore[4] compared his calculated results with the data by Demuth *et al.*[10] on the Ni(001) face and obtained good agreement in the absolute reflectivities. However, when he compared his calculated results for Ni(111) with data taken by others,[25,26] he found that theory and experiment differed in absolute reflectivities by as much as a factor of 8. This led him to the conclusion that the same dynamical model would not give absolute reflectivities in agreement with experiment on the two faces of nickel. A cursory check on the now available data by Demuth and Rhodin for Ni(111)[11,12] with Laramore's calculated results[4] shows rather good agreement in absolute reflectivities between theory and experiment on the (111) face. For example, the peak at $E = 130$ eV, $\theta = 6°$, $\varphi = 0°$ is about 1.8% (experiment, Demuth and Rhodin[11,12]) compared to 1.9% (theory, Laramore[4]), and 0.3% (experiment, Ngoc *et al.*[26]). Experimentally measured reflectivities are extremely sensitive to the degree of surface order and the way in which crystal samples are prepared. Two different sample preparation procedures can produce crystals with very different measured absolute reflectivites. An experimentalist who follows the same cleaning procedure in preparing different faces of a material has a higher, but not guaranteed, chance of obtaining the different crystal faces with relatively similar surface order (or disorder). However, until there is a reliable way to quantitatively monitor surface order on different crystal faces, it is perhaps not very useful to directly compare absolute reflectivities since the calculations assume a perfectly ordered surface structure. A more useful scheme is as follows. We define a number by |(measured absolute reflectivity)/(calculated absolute reflectivity)| = S. If, from comparisons between theory and experiment on different crystal faces, S is found to vary only slightly from face to face, then we may conclude that the data were taken on crystal faces with comparable degrees of surface order. The data by Demuth and co-workers[10-12] on the three faces of nickel seem to have that quality.

ACKNOWLEDGMENTS

It is a pleasure to acknowledge stimulating discussions with Dr. G. P. Alldredge who worked closely with us on the layer-dependent mean-square vibration amplitudes problem. Special thanks are to Dr. F. W. deWette for his interest and support of this work. One of us (S. Y. T.) is also grateful to the research group of F. W. deWette for enabling him to spend two weeks at the University of Texas, Austin as a research consultant during the course of this work.

*Work supported in part by the Air Force Office of Scientific Research (AFSC) under Grant No. AFOSR-71-1973 and in part by the National Science Foundation, Grant No. GH-40626.

†Permanent address,

[1] S. Y. Tong, T. N. Rhodin, and R. H. Tait, Phys. Rev. B 8, 421 (1973); Phys. Rev. B 8, 430 (1973).
[2] G. E. Laramore and C. B. Duke, Phys. Rev. B **5**, 267 (1972).
[3] D. W. Jepsen, P. M. Marcus, and F. Jona, Phys. Rev. B **6**, 3684 (1972).
[4] G. E. Laramore, Phys. Rev. B **8**, 515 (1973).
[5] L. L. Kesmodel, J. B. Pendry, and S. Y. Tong (unpublished).
[6] J. E. Demuth, D. W. Jepsen and P. M. Marcus, Seventh LEED Seminar, San Diego, Calif. 1973 (unpublished).
[7] F. Jona, IBM J. Res. Dev. **14**, 444 (1970).
[8] R. H. Tait, S. Y. Tong, and T. N. Rhodin, Phys. Rev. Lett. **28**, 553 (1972).
[9] S. Y. Tong, T. N. Rhodin, and R. H. Tait, Surf. Sci. 34, 457 (1973).
[10] J. E. Demuth, S. Y. Tong, and T. N. Rhodin, J. Vac. Sci. Technol. **9**, 639 (1972).
[11] J. E. Demuth, Ph.D. thesis (Cornell University, 1973) (unpublished).
[12] J. E. Demuth and T. N. Rhodin (unpublished).
[13] S. Andersson and J. B. Pendry, J. Phys. C **5**, L41 (1972).
[14] S. Andersson and J. B. Pendry, J. Phys. C (to be published).

[15]C. B. Duke, G. E. Laramore and J. B. Theeten (unpublished).
[16]A. Ignatiev, T. N. Rhodin, S. Y. Tong, B. I. Lundqvist, and J. B. Pendry, Solid State Commun. **9**, 1851 (1971).
[17]S. Y. Tong, T. N. Rhodin, and A. Ignatiev, Phys. Rev. B **8**, 906 (1973).
[18]B. C. Clark, R. Herman, and R. F. Wallis, Phys. Rev. **133**, A1188 (1964).
[19]A. A. Maradudin and J. Melngailis, Phys. Rev. **133**, A1188 (1964).
[20]R. E. Allen and F. W. deWette, Phys. Rev. **179**, 873 (1969).
[21]R. E. Allen, F. W. DEWette, and A. Rahman, Phys. Rev. **179**, 887 (1969).
[22]R. E. Allen and F. W. deWette, Phys. Rev. **188**, 1320 (1969).
[23]S. Andersson, Ph.D. thesis (Chalmers University of Technology, 1970) (unpublished).
[24]S. Andersson and B. Kasemo, Surf. Sci. **25**, 273 (1971).
[25]M. G. Lagally, T. C. Ngoc, and M. B. Webb, J. Vac. Sci. Technol. **9**, 645 (1972).
[26]T. C. Ngoc, M. G. Lagally, and M. B. Webb, Surface Sci. (to be published).
[27]R. L. Park and H. E. Farnsworth, J. Appl. Phys. **37**, 295 (1966).
[28]R. L. Park and H. E. Farnsworth, J. Chem. Phys. **40**, 2354 (1964).
[29]R. L. Park and H. E. Farnsworth, Surf. Sci. **2**, 527 (1964).
[30]J. L. Beeby, J. Phys. C **1**, 82 (1968).
[31]S. Y. Tong and T. N. Rhodin, Phys. Rev. Lett. **26**, 711 (1971).
[32]S. Y. Tong, G. E. Laramore, and T. N. Rhodin, Phys. Rev. (to be published).
[33]L. L. Kesmodel, S. Y. Tong, and G. P. Alldredge (unpublished).
[34]For expansions of the Debye-Waller factor in terms of three coefficient functions by curve fitting to three scattering angles, see Ref. 4.
[35]S. Wakoh, J. Phys. Soc. Jap. **20**, 1984 (1965).
[36]J. P. Pendry, J. Phys. C **4**, 2501 (1971); J. Phys. C **4**, 2514 (1971).
[37]J. B. Pendry, Phys. Rev. Lett. **27**, 856 (1971).